

Static-field ionization model of He-like ions for diagnostics of light field intensity

Erik Lötstedt,^{1,*} Marcelo F. Ciappina,^{2,3} and Kaoru Yamanouchi¹

¹*Department of Chemistry, School of Science,
The University of Tokyo, 7-3-1 Hongo,
Bunkyo-ku, Tokyo 113-0033, Japan*

²*Institute of Physics of the ASCR, ELI-Beamlines project,
Na Slovance 2, 182 21 Prague, Czech Republic*

³*ICFO – Institut de Ciències Fotoniques,
The Barcelona Institute of Science and Technology, 08860 Castelldefels (Barcelona)*

(Dated: January 12, 2022)

Abstract

We study static-field ionization of He-like ions with nuclear charge number in the range of $2 \leq Z \leq 36$. Both the tunneling and over-the-barrier regimes are considered. We calculate the ionization rates by three approximate methods: a fitting formula based on the Perelemov-Popov-Terent'ev (PPT) formula, a perturbative expansion in powers of $1/Z$, and a single-active electron approximation, and compare them with reference ionization rates computed by the multiconfiguration time-dependent Hartree-Fock (MCTDHF) approach. The relative deviation of the rates computed by the PPT-based fitting formula and the third-order perturbation theory from the rates computed by the MCTDHF approach is found to be around 10%. We discuss quantitatively the contribution from the exchange interaction during the ionization by comparing the single-active electron rates and the reference rates in which multielectron effects are included. We find that a single-active electron approximation, where the exchange interaction is neglected, results in the overestimation of the ionization rates by 30% for He and 2% for He-like Kr, showing that the magnitude of the effect of the exchange interaction scales approximately as $1/Z$.

I. INTRODUCTION

Strong-field ionization of atoms has been proposed as a means of estimating the peak intensity of laser pulses having an intensity of $I > 10^{20}$ W/cm² [1–5]. Such ultra-intense laser pulses are becoming available at several facilities worldwide, two examples being the ELI Beamlines [6] and the Shanghai super-intense ultrafast laser facility [7]. In [3, 4], it was shown that the relative yields of different ionic charge states are highly sensitive to the peak intensity of the laser pulse and that the final charge state distribution can be used to estimate the laser field intensity at the beam focus. Moreover, it was concluded in [4] that the highest accuracy can be achieved in the determination of the laser field intensity when the ionization yields of He- and H-like ions are adopted.

In order to relate quantitatively the measured ion yield to the laser field intensity, it is necessary to simulate the ion yields using reliable formulas for the tunneling and over-the-barrier (OTB) static-field ionization rates. Ionization rates for H-like ions are well established through the tunneling-rate formula originally derived by Smirnov and Chibisov

* lotstedt@chem.s.u-tokyo.ac.jp

[8], which has also been referred to as the Perelemov-Popov-Terent'ev (PPT) formula [9–11] or the Ammosov-Delone-Krainov (ADK) [12] formula, providing reliable estimates of the ionization rates in the tunneling regime. Within the single-active electron approximation, the ADK theory has been extended to molecular systems [13–17]. Attempts have also been made to include many-electron effects in static-field tunneling ionization [18, 19]. When the field intensity is sufficiently weak, the weak-field asymptotic theory (WFAT) [20] provides a rigorous expansion of the pre-exponential factor in the tunneling rate in powers of the field strength. The WFAT has been extended to many-electron systems [21–24] and has been applied to molecular ionization [25, 26]. In [24], the WFAT was applied to He-like ions for an arbitrary value of the nuclear charge number Z .

In order to estimate a static-field ionization rate in the OTB regime, we need to adopt numerical methods because there are no analytical formulas available. Static-field ionization rates of H [27–29], He [30–32] and H₂ [33] have been studied numerically by the complex scaling methods, which have also been applied to many-electron atoms [34] and diatomic and triatomic molecules (CO, N₂, O₂, CO₂) [35, 36]. In Ref. [37], static-field ionization rates of He were obtained by real-time integration of the time-dependent Schrödinger equation (TDSE). However, to the best of our knowledge, no numerical studies have been reported so far on the tunneling and OTB ionization rates of He-like ions. It has been awaited that reliable methods for estimating ionization rates for He-like ions valid in both the tunneling and the OTB regimes are established, so that the scheme for estimating the laser field intensity proposed in [3] will be realized. The advantage of treating He-like ions is that the effect of the electron-electron correlation in the static-field ionization processes can be varied systematically by the change in the nuclear charge number Z .

In the present study, we investigate the static-field tunneling and OTB ionization of He-like ions with the nuclear charge number Z in the range of $2 \leq Z \leq 36$. We compare (i) ionization rates obtained by the PPT formula, (ii) ionization rates obtained by a PPT-based fitting formula proposed by Tong and Lin [38], (iii) ionization rates calculated by a perturbative expansion in powers of $1/Z$, (iv) ionization rates calculated by the single-active electron (SAE) approximation, and (v) reference ionization rates obtained by the multiconfiguration time-dependent Hartree-Fock (MCTDHF) method [39, 40], in which the electron-electron interaction is fully accounted for. We compare the deviation of the approximate rates from the rates calculated by the MCTDHF method, and find that both the approach (ii) and the

approach (iii) result in rates which deviate by about 10% from the MCTDHF rates. Considering that the approach (ii) is easier to be applied than the approach (iii), we recommend the approach (ii) to be used in the evaluation of static-field ionization rates of He-like ions.

II. THEORY

In this section, we describe the theoretical methods that we employ in the present study. Atomic units (a.u.) are used throughout the paper unless otherwise indicated. For the conversion from a.u. to SI units, we have $1 \text{ a.u.} = 4.134 \times 10^{16} \text{ s}^{-1}$ for ionization rates, and $1 \text{ a.u.} = 5.142 \times 10^{11} \text{ V/m}$ for electric fields.

In the calculation of the static-field ionization rates, we employ the nonrelativistic TDSE. Although we will present results for the ionization of He-like ions with the large charge number Z up to $Z = 36$, where the intensity of a laser field required for ionization reaches 10^{22} W/cm^2 , it has been shown that the ionization process itself is essentially nonrelativistic for ions with $Z < 20$ [3, 41]. As long as the ionization potential I_p of an atom is much smaller than the rest energy of an electron, $I_p \ll c^2$, where $c \approx 137 \text{ a.u.}$, the relativistic effects in the ground state wave function can be neglected. Using $I_p \approx Z^2/2$ for large Z , we see that $I_p \ll c^2$ is satisfied even for $Z = 36$ because $I_p/c^2 = 36^2/(2c^2) \approx 0.03$.

The static-field ionization rates obtained in this study can be used to estimate the ionization probability in a low-frequency laser field as long as the static-field ionization rates can be used as instantaneous ionization rates. This procedure is valid if the Keldysh parameter $\gamma = \sqrt{2I_p}\omega/F$, where ω is the angular frequency of the laser field and F is the peak field strength, is smaller than 1 [3, 42]. In this study, we consider values of F so that $\gamma < 1$. For example, for He ($Z = 2$), we consider $F \approx 0.4 \text{ a.u.}$, which gives $\gamma = 0.2$ assuming $\omega = 0.057 \text{ a.u.}$ (corresponding to a wavelength of 800 nm), and for He-like Kr ($Z = 36$), we consider $F \approx 2 \times 10^3 \text{ a.u.}$, which gives $\gamma = 0.001$ at $\omega = 0.057 \text{ a.u.}$

A. Z -scaling

The TDSE for a He-like ion with the charge number Z in a static electric field $\mathbf{F} = F\hat{\mathbf{z}}$ reads

$$i\frac{\partial}{\partial t}\Psi(\mathbf{r}_1, \mathbf{r}_2, t) = [H + F(z_1 + z_2)]\Psi(\mathbf{r}_1, \mathbf{r}_2, t), \quad (1)$$

where $\mathbf{r}_i = (x_i, y_i, z_i)$ is the coordinate of the i th electron, and the field-free Hamiltonian is defined as

$$H = \sum_{i=1,2} \left(-\frac{1}{2} \frac{\partial^2}{\partial \mathbf{r}_i^2} - \frac{Z}{r_i} \right) + \frac{1}{r_{12}}, \quad (2)$$

with $r_{12} = |\mathbf{r}_1 - \mathbf{r}_2|$. After scaling the spatial coordinates and time according to [43]

$$\mathbf{r}_i = \frac{2\mathbf{r}'_i}{Z}, \quad t = \frac{4t'}{Z^2}, \quad (3)$$

and rewriting the TDSE (1) in the scaled coordinates, we obtain

$$i \frac{\partial}{\partial t'} \Psi'(\mathbf{r}'_1, \mathbf{r}'_2, t') = [H' + F'(z'_1 + z'_2)] \Psi'(\mathbf{r}'_1, \mathbf{r}'_2, t'), \quad (4)$$

where

$$H' = \sum_{i=1,2} \left(-\frac{1}{2} \frac{\partial^2}{\partial \mathbf{r}'_i{}^2} - \frac{2}{r'_i} \right) + \frac{2}{Z} \frac{1}{r'_{12}}, \quad (5)$$

and $\Psi'(\mathbf{r}'_1, \mathbf{r}'_2, t') = (2/Z)^3 \Psi(\mathbf{r}_1, \mathbf{r}_2, t)$. The scaling of the amplitude of the electric field is

$$F' = \frac{8}{Z^3} F. \quad (6)$$

The transformation described above implies that a He-like atomic ion with the charge number Z is described by the same TDSE as He and that the electron-electron interaction is scaled by $2/Z$, indicating that the relative magnitude of the electron-electron interaction compared to the electron-nucleus interaction decreases as Z increases.

For the ionization rate, we have the following scaling relation,

$$\Gamma(F) = \frac{Z^2}{4} \Gamma'(F'), \quad (7)$$

where $\Gamma(F)$ is the rate we obtain by solving Eq. (1) at the field F and $\Gamma'(F')$ is the rate we obtain by solving Eq. (4) at the field $F' = 8F/Z^3$.

In the following part of the paper, symbols with a prime always refer to the quantities in the transformed system (4) and symbols without a prime refer to those in the original system (1).

B. MCTDHF

In order to solve the scaled TDSE (4) numerically, we employ the MCTDHF method [39, 40, 44–47]. In the MCTDHF method, the two-electron wave function is expanded in

terms of time-dependent Slater determinants $\|\phi'_i(t')\alpha\phi'_j(t')\beta\|$,

$$\Psi'(t') = \sum_{i,j=1}^M C'_{ij}(t') \|\phi'_i(t')\alpha\phi'_j(t')\beta\|, \quad (8)$$

where $\phi'_i(\mathbf{r}', t')$ is a time-dependent spatial orbital, M is the total number of orbitals, α (spin up) and β (spin down) are spin functions, and $C'_{ij}(t')$ is a time-dependent configuration-interaction (CI) coefficient. The equations of motion for the spin-orbitals and the CI coefficients are derived by applying the time-dependent variational principle [39, 40]. The MCTDHF method has previously been applied to He in the calculation of two-photon ionization probabilities [48], high-harmonic spectra [49], above-threshold photoelectron spectra [50], and strong-field excitation probabilities [51].

It should be noted here that the MCTDHF method is different from other commonly employed close-coupling approaches [37, 52–54] in that products of single-electron orbitals are used in the expansion of the time-dependent wave function, while in [37, 52–54] the two-electron wave function is expanded in terms of two-electron radial basis functions multiplied with two-electron spherical harmonics.

We solve the MCTDHF equations of motion in the same way as described in [51, 55]. The details of the numerical implementation of the MCTDHF method are summarized in Appendix A.

In order to obtain the ionization rate Γ , we solve the scaled TDSE (4) starting from the ground state, $\Psi'(t' = 0) = \Psi'_0$, and calculate the time-dependent population of the ground state, $p_0(t') = |\langle \Psi'_0 | \Psi'(t') \rangle|^2$. For $t' < t'_0$ ($t'_0 \approx 50$ a.u.), $p_0(t')$ oscillates due to the transitions to the excited states induced by the sudden turn-on of the static field. For $t' > t'_0$, $p_0(t')$ decreases exponentially and can be fitted to an exponential function $e^{-\Gamma' t' - q'}$ with the constant Γ' , representing the scaled ionization rate, and q' [32]. After the simulations with different values of the static field F' , the scaled field-dependent ionization rate $\Gamma'(F')$ is obtained, from which the ionization rate of a He-like ion is calculated by the scaling of Eq. (7). However, if the ionization rate is very large or very small, it becomes difficult to obtain the ionization rate by this approach because $p_0(t')$ cannot be fitted well to $e^{-\Gamma' t' - q'}$ when it changes too slowly or too rapidly. Consequently, the scaled fields need to be limited practically in the range of $0.1 \lesssim F' \lesssim 1$ a.u.

C. Perturbation theory

In the limit of $Z \rightarrow \infty$, the scaled Eq. (4) decouples and becomes an equation for two independent He^+ ions. Therefore, in the large Z limit, the scaled ionization rate for a He-like ion can be expressed as

$$\Gamma'(F') \underset{Z \rightarrow \infty}{=} 8\Gamma_{\text{H}}(F), \quad (9)$$

where $\Gamma_{\text{H}}(F)$ is the ionization rate of H evaluated at the unscaled field of $F = F'/8$.

For finite but large values of Z , we can treat the electron-electron interaction term $2/(Zr'_{12})$ in the scaled Hamiltonian (5) as a perturbation, and evaluate corrections using perturbation theory. By inserting the expansions

$$\Psi'(\mathbf{r}'_1, \mathbf{r}'_2) = \sum_{n=0}^{\infty} \frac{\chi'_n(\mathbf{r}'_1, \mathbf{r}'_2)}{Z^n} \quad (10)$$

and

$$\epsilon' = \sum_{n=0}^{\infty} \frac{\epsilon'_n}{Z^n} \quad (11)$$

into the eigen equation,

$$H'(e^{i\Theta}\mathbf{r}'_1, e^{i\Theta}\mathbf{r}'_2)\Psi'(\mathbf{r}'_1, \mathbf{r}'_2) = \epsilon'\Psi'(\mathbf{r}'_1, \mathbf{r}'_2), \quad (12)$$

where $H'(e^{i\Theta}\mathbf{r}'_1, e^{i\Theta}\mathbf{r}'_2)$ is the scaled complex-rotated Hamiltonian (5) [56], we derive equations relating χ'_n and ϵ'_n at different orders of $1/Z$. Throughout our calculations we use the complex rotation parameter $\Theta = 0.2$. The equations up to the third order are given in Appendix B1. After the field-dependent correction terms $\epsilon'_n(F')$ for the eigenvalue of the ground state are calculated, the unscaled ionization rate corrected up to the order N at a given value of Z is given by

$$\Gamma_{\text{pert}}^N(F') = \frac{Z^2}{4} \sum_{n=0}^N \frac{\lambda'_n(F')}{Z^n}, \quad (13)$$

with

$$\lambda'_n(F') = -2 \text{Im} [\epsilon'_n(F')]. \quad (14)$$

It should be noted here that the correction terms ϵ'_n contain corrections both to the eigenenergy (the real part of ϵ'_n) and to the ionization rate (the imaginary part of ϵ'_n) of the ground state and that the rate given by Eq. (13) contains contributions from all orders in the field F' , because the interaction with the field is included in the zeroth-order Hamiltonian.

D. Single-active electron approximation

In the single-active electron approximation (SAE), the SAE Hamiltonian reads

$$H'_{\text{SAE}}(\mathbf{r}') = -\frac{1}{2} \frac{\partial^2}{\partial \mathbf{r}'^2} + V(\mathbf{r}') + F'z', \quad (15)$$

where $V(\mathbf{r}')$ is an effective potential. We consider below the SAE approximation to the scaled TDSE (4).

A commonly used effective potential for He-like ions reads [32]

$$V_1(\mathbf{r}') = -\frac{2 - \frac{2}{Z} + \frac{2}{Z}e^{-\zeta' r'}}{r'}, \quad (16)$$

where the parameter ζ' is adjusted so that the absolute value of the ground state energy becomes equal to the ionization potential of the corresponding two-electron system. For He, we additionally consider a polarization potential in order to model the effect of the electric field on the inner electron, that is, the electron left bound after the ejection of the other electron. The polarization potential is thus defined as

$$V_{\text{pol}}(\mathbf{r}) = -F\alpha_{\text{He}^+} \cos \theta \frac{1 - e^{-\eta r} (1 + \eta r + \frac{1}{2}\eta^2 r^2)}{r^2}, \quad (17)$$

where θ is the polar angle, $\alpha_{\text{He}^+} = 9/2^5 \approx 0.28$ a.u. is the polarizability of He^+ [57], and η is a parameter describing the range of the polarization potential. The polarization potential is constructed so that $V_{\text{pol}}(r \rightarrow \infty) = -F\alpha_{\text{He}^+} \cos \theta / r^2$ and $V_{\text{pol}}(r \rightarrow 0) = 0$. Finally, the full effective SAE potential including $V_{\text{pol}}(\mathbf{r})$ reads

$$V_2(\mathbf{r}) = V_1(\mathbf{r}) + V_{\text{pol}}(\mathbf{r}). \quad (18)$$

The parameter η is fixed so that two times the polarizability of the single active electron matches the polarizability of He.

For He, we have also investigated a more complicated SAE potential of the form $V_3(r) = -[1 + e^{-\zeta_1 r} + \beta r(r - q)e^{-\zeta_2 r}]/r$, where the parameters ζ_1 , ζ_2 , β , and q are determined by the minimization of the difference between the ground state single-electron density obtained by the SAE approximation and the ground state single-electron density obtained by the MCT-DHF method. The difference between the ionization rates obtained by using the potential $V_3(r)$ and the ionization rates obtained by the potential $V_1(r)$ defined in Eq. (16) was found to be small. Indeed, the relative difference is smaller than 4% for fields $0.2 \leq F \leq 0.6$ a.u.

We therefore conclude that the ionization rate is not sensitive to a small variation of the form of the SAE potential as long as the ionization potential is well reproduced.

The ionization rates in the SAE approximation are obtained by calculating the lowest energy eigenvalue ϵ'_{SAE} of the complex-rotated Hamiltonian $H'_{\text{SAE}}(e^{i\Theta}\mathbf{r}')$ [56],

$$H'_{\text{SAE}}(e^{i\Theta}\mathbf{r}')\psi'_{\text{SAE}}(\mathbf{r}') = \epsilon'_{\text{SAE}}\psi'_{\text{SAE}}(\mathbf{r}'), \quad (19)$$

with $\Theta = 0.2$. From the complex-valued eigenvalue ϵ'_{SAE} , we obtain the scaled tunneling rate for a two-electron atom as

$$\Gamma'_{\text{SAE}} = -4 \text{Im}(\epsilon'_{\text{SAE}}), \quad (20)$$

and the unscaled original rate by the scaling relation (7). Note that there is an additional factor of 2 in Eq. (20) originating from the indistinguishability of the two electrons.

In addition to the SAE approximation, we also discuss results obtained by the frozen core (FC) model of He [32],

$$\begin{aligned} \Psi_{\text{FC}}(\mathbf{r}_1, \mathbf{r}_2, t) = & c_0(t) \Psi_0^{\text{He}}(\mathbf{r}_1, \mathbf{r}_2) \\ & + \frac{1}{\sqrt{2}} \left[\psi_0^{\text{He}^+}(\mathbf{r}_1) \phi(\mathbf{r}_2, t) + \phi(\mathbf{r}_1, t) \psi_0^{\text{He}^+}(\mathbf{r}_2) \right], \end{aligned} \quad (21)$$

where $\Psi_0^{\text{He}}(\mathbf{r}_1, \mathbf{r}_2)$ is the ground state wave function of He, and $\psi_0^{\text{He}^+}(\mathbf{r})$ is the ground state wave function of He^+ . We can derive equations of motion for $c_0(t)$ and $\phi(\mathbf{r}, t)$ by inserting $\Psi_{\text{FC}}(\mathbf{r}_1, \mathbf{r}_2, t)$ into the TDSE (1). We obtain the ionization rate Γ_{FC} by fitting the decreasing ground-state norm $|c_0(t)|^2$ to an exponential function $e^{-\Gamma_{\text{FC}}t - q}$. In the context of static-field ionization of He, the ansatz (21) was introduced by Scrinzi [32], and similar models have been successfully used in the numerical simulations of many-electron molecules in strong fields [36, 58–60]. The wave function (21) describes a single active electron with the ejected part of the wave function given by $\phi(\mathbf{r}, t)$, and includes the exchange interaction of the ejected electron with the He^+ core, differently from the SAE model.

III. RESULTS

A. Comparison of MCTDHF rates and PPT rates

In Fig. 1, we show the comparison between the ionization rates Γ calculated with the MCTDHF method and the ionization rates Γ_{PPT} calculated with the PPT formula [4, 9, 11].

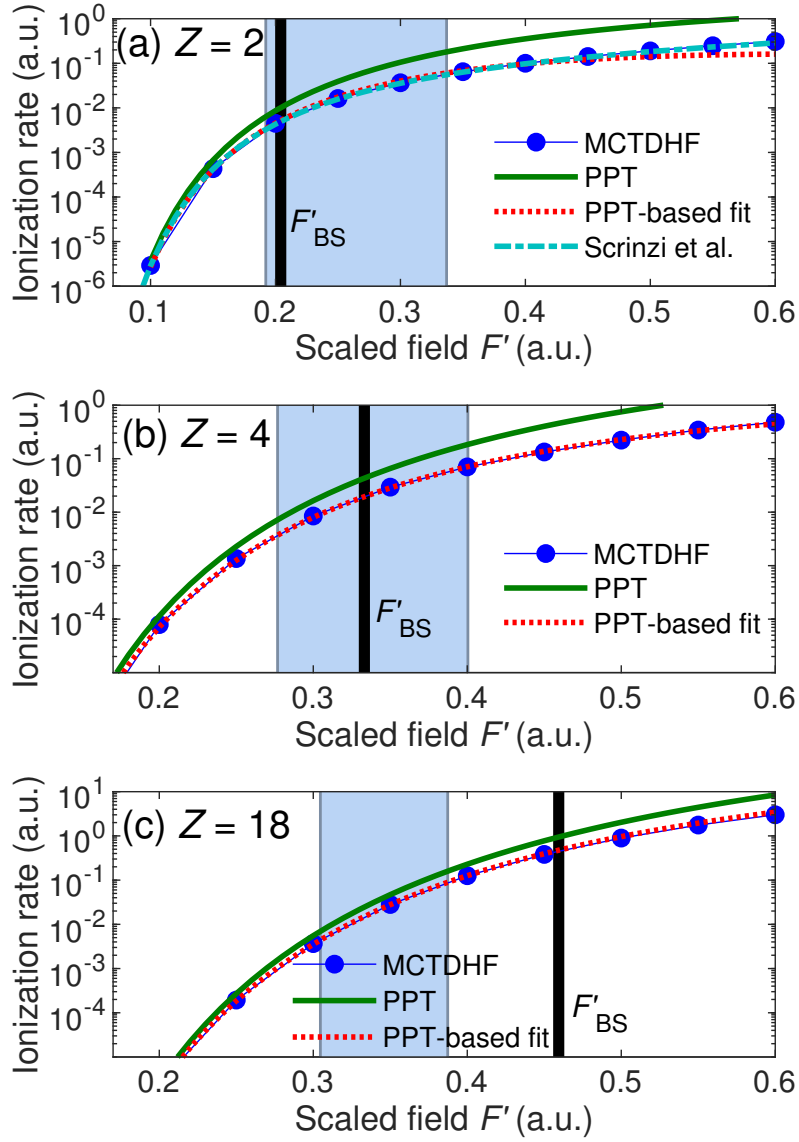


FIG. 1. Ionization rates $\Gamma = Z^2 \Gamma'/4$ calculated with the MCTDHF method for (a) He, (b) He-like Be ($Z = 4$), and (c) He-like Ar ($Z = 18$) are shown with filled circles. The ionization rates are shown as a function of the scaled field $F' = 8F/Z^3$. Comparisons are made with the ionization rates calculated using the PPT formula [solid line; see Eq. (C1)] and the PPT-based fitting formula suggested in [38] [dotted line; see Eq. (22)]. In panel (a), the dash-dotted line shows the results obtained by Scrinzi, Geissler and Brabec in [31]. The scaled barrier suppression field F'_{BS} is indicated with a vertical solid line. The blue shaded area indicates the interval where the ionization probability during one laser cycle P_{ion} [defined in Eq. (25)] is in the range between 10% and 90%. In terms of peak laser field intensities, $F' = 0.4$ a.u. corresponds to 5.6×10^{15} W/cm² for $Z = 2$, 3.6×10^{17} W/cm² for $Z = 4$, and 3.0×10^{21} W/cm² for $Z = 18$.

The PPT formula employed in this study is given by Eq. (C1) in Appendix C. Note that the PPT rate is defined with an additional factor of 2, originating from the fact that two electrons contribute to the total ionization rate. For He ($Z = 2$), a comparison is made with the rates Γ_{SGB} calculated by Scrinzi, Geissler and Brabec [31] using the complex scaling method for a correlated two-electron wave function.

Also shown in Fig. 1 are the results obtained by the PPT-based fitting formula for the ionization rate suggested by Tong and Lin [38],

$$\Gamma_{\text{fit}}(F) = \Gamma_{\text{PPT}}(F)\Lambda_{\alpha}(F), \quad (22)$$

where

$$\Lambda_{\alpha}(F) = \exp \left[-\alpha \frac{(Z-1)^2}{I_p} \frac{F}{(2I_p)^{\frac{3}{2}}} \right] \quad (23)$$

is an empirical correction factor, and I_p is the ionization potential. For the I_p of He-like ions, we use the expression given in Eq. (C5) in Appendix C. We note that the expression (22) should be viewed as a formula with which the ionization rates obtained by ab initio methods can be fitted. In [38], the parameter α in the empirical correction factor $\Lambda_{\alpha}(F)$ was suggested to be $\alpha = 7$ for He, but the values for other He-like ions were not given. We derive α by a least-squares fit of the PPT-based fitting formula $\Gamma_{\text{fit}}(F)$ to the rate obtained by the MCTDHF method, using the ionization rates in the range of $0.2 \leq F' \leq 0.4$ a.u. We obtain $\alpha = 7.12$ for $Z = 2$, $\alpha = 7.14$ for $Z = 4$, and $\alpha = 5.62$ for $Z = 18$. The applicability of the PPT-based fitting formula (22) has been confirmed previously in the case of strong-field ionization of H, where the PPT-based fitting formula (22) with $\alpha = 6$ differs from accurate numerical ionization rates by less than 10% for the unscaled fields of $F < 0.125$ a.u. [38].

Because $\Lambda_{\alpha}(F)$ becomes exponentially small as F increases, the formula (22) cannot be valid when F becomes too large, but, as can be seen in Fig. 1, it is remarkably accurate as long as the field strength is in the tunneling regime as well as in the OTB regime below the field strength at $F \approx 2F_{\text{BS}}$, where the barrier-suppression field F_{BS} is defined as

$$F_{\text{BS}} = \frac{I_p^2}{4(Z-1)}. \quad (24)$$

The quantity $Z - 1$ represents the residual charge with which the ejected electron interacts. We regard that the field strength is in the tunneling regime when $F < F_{\text{BS}}$ and that the field strength is in the OTB regime when $F > F_{\text{BS}}$. We show F_{BS} in Fig. 1 as a thick vertical

line. The scaled barrier-suppression field $F'_{\text{BS}} = 8F_{\text{BS}}/Z^3$ is defined according to the scaling relation, Eq. (6).

In [61], an improved empirical correction factor $\Lambda_{\alpha_1\alpha_2\alpha_3}(F) = \exp(-\alpha_1 F^2/F_{\text{BS}}^2 - \alpha_2 F/F_{\text{BS}} - \alpha_3)$ to the PPT formula with the three fitting parameters $\alpha_1, \alpha_2, \alpha_3$ was proposed. However, we employ the original correction factor introduced in [38], in which only one fitting parameter, α , is used, for its simplicity.

In order to relate the static-field rates to the probability of ionization in an oscillating laser field, we evaluate the ionization probability P_{ion} during one optical cycle of a laser field with the peak amplitude F and the angular frequency ω as

$$P_{\text{ion}}(F) = 1 - \exp \left[-\frac{1}{\omega} \int_0^{2\pi} \Gamma(|F \sin s|) ds \right], \quad (25)$$

where $\omega = 0.057$ a.u., corresponding to a wavelength of 800 nm, is chosen. The expression (25) for the ionization probability of a He-like ion in a laser field is valid under the assumption of a slowly varying field. In Fig. 1, the interval where P_{ion} fulfills $0.1 \leq P_{\text{ion}} \leq 0.9$ is indicated by the area shaded with light blue color.

We can see in Fig. 1 that the standard PPT formula overestimates the ionization rates compared with the reference MCTDHF rates, even though the extent of the overestimation becomes smaller for the larger values of Z . On the other hand, the rates obtained by the PPT-based fitting formula agree well with the MCTDHF rates. For $Z = 2$, the relative deviation takes the values of $|\Gamma_{\text{fit}} - \Gamma|/\Gamma < 0.1$ when $F' \leq 0.4$ a.u. and $|\Gamma_{\text{fit}} - \Gamma|/\Gamma < 0.5$ when $F' \geq 0.4$ a.u. For $Z = 4$, we have $|\Gamma_{\text{fit}} - \Gamma|/\Gamma < 0.1$ when $F' \geq 0.25$ a.u. For $Z = 18$, $|\Gamma_{\text{fit}} - \Gamma|/\Gamma < 0.1$ when $0.25 \leq F' \leq 0.5$ a.u. and $|\Gamma_{\text{fit}} - \Gamma|/\Gamma < 0.15$ when $F' > 0.5$ a.u. This shows that the PPT-based fitting formula has a relative accuracy of 10% or better in the electric field range where the ionization probability is substantially large but below the saturation ($0.1 < P_{\text{ion}} < 0.9$), corresponding to the range indicated by light blue color in Fig. 1. An accurate formula for the ionization rate in this field strength range is crucial for the simulation of the ion yields required in the intensity estimation scheme proposed in [3, 4].

In the case of He, the MCTDHF rates and the rates Γ_{SGB} calculated by Scrinzi, Geissler, and Brabec [31] are in good agreement with each other, which confirms the validity of the MCTDHF method for calculating static-field ionization rates. The relative deviation takes the values of $|\Gamma_{\text{SGB}} - \Gamma|/\Gamma_{\text{SGB}} < 0.05$ when $F' \leq 0.5$ a.u. and $|\Gamma_{\text{SGB}} - \Gamma|/\Gamma_{\text{SGB}} < 0.08$ when

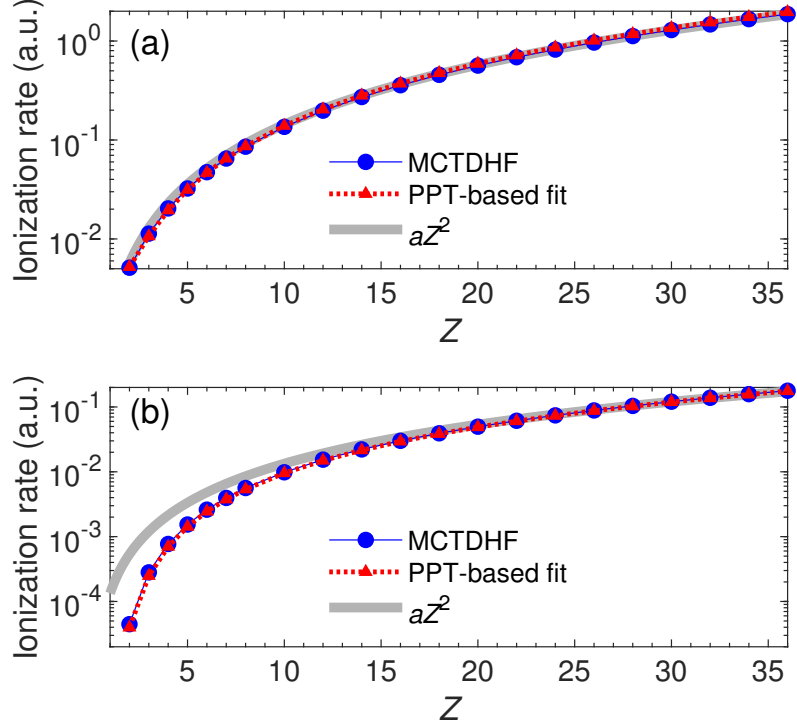


FIG. 2. (a) Ionization rate $\Gamma = Z^2 \Gamma' / 4$ at $F = F_{BS}$ calculated with the MCTDHF method (blue solid circles), the rate Γ_{fit} calculated with the PPT-based fitting formula (red triangles) and a fit of Γ to a quadratic function aZ^2 with $a = 1.4 \times 10^{-3}$ (thick solid gray line) are shown as a function of Z . (b) Ionization rates evaluated at $F = (2I_p)^{3/2} \times 0.05$, such that the reduced field $\tilde{F} = 0.05$ a.u. The coefficient a in the quadratic fit is $a = 1.3 \times 10^{-4}$.

$F' > 0.5$ a.u. The small discrepancy between our results and the results obtained in [31] can be ascribed to the difference in the method used in the calculations. In [31], the ionization rates were obtained by the complex scaling of a two-electron wave function expanded in terms of explicitly correlated basis functions. The rates for He obtained by the MCTDHF method are also in good agreement with the ionization rates reported by Parker et al. in [37], where the TDSE was integrated in real time and the ionization rate was obtained by monitoring the decay of the norm of the wave function in a sphere whose radius is 18 a.u. around the atomic core. For comparison, numerical values of the ionization rates for He obtained by the MCTDHF method are listed together with the ionization rates reported in Ref. [31] and Ref. [37] in Appendix D.

To further assess the accuracy of the PPT-based fitting formula, we evaluate the ionization rate as a function of Z at two different values of F . In Fig. 2(a), we show the ionization rate

TABLE I. Parameter α adopted in the PPT-based fitting formula (22).

Z	α	Z	α	Z	α	Z	α
2	7.12	8	6.23	20	5.57	32	5.41
3	7.52	10	6.00	22	5.53	34	5.40
4	7.14	12	5.88	24	5.49	36	5.39
5	6.84	14	5.77	26	5.47		
6	6.58	16	5.68	28	5.45		
7	6.38	18	5.62	30	5.43		

evaluated at the barrier-suppression field F_{BS} for $Z \leq 36$. We compare the rate $\Gamma(F = F_{\text{BS}})$ calculated with the MCTDHF method and the rate $\Gamma_{\text{fit}}(F = F_{\text{BS}})$ calculated with the PPT-based fitting formula defined by Eq. (22). For each value of Z , α is obtained by fitting $\Gamma_{\text{fit}}(F')$ to the ionization rates $\Gamma(F')$ calculated by the MCTDHF method for the scaled fields in the range of $0.2 \leq F' \leq 0.4$ a.u. The numerical values of α are given in Table I. For reference, we provide numerical values of the ionization rates in the Supplemental material [62].

The relative difference between Γ and Γ_{fit} , defined as $|\Gamma_{\text{fit}}(Z) - \Gamma(Z)|/\Gamma(Z)$, is less than 6% for all $Z \geq 2$. It can also be seen in Fig. 2(a) that the Z -dependence of the ionization rate Γ at $F = F_{\text{BS}}$ is quadratic to a good approximation. This means that the scaled rate $\Gamma'(F'_{\text{BS}})$ is almost independent of Z because Γ is scaled by $Z^2/4$ with respect to Γ' as shown in the relation (7). A fit of Γ to the function $\Gamma_{\text{fit}} = aZ^2$ gives $a \approx 1.4 \times 10^{-3}$. As can be seen in Fig. 2(a), $\Gamma_{\text{fit}} = aZ^2$ agrees well with the rate obtained by the MCTDHF method. For Z in the range $2 \leq Z \leq 10$, the relative error of the quadratic fit is $|\Gamma_{\text{fit}}(Z) - \Gamma(Z)|/\Gamma(Z) < 0.15$, and for $Z > 10$, it becomes $|\Gamma_{\text{fit}}(Z) - \Gamma(Z)|/\Gamma(Z) < 0.05$.

In Fig. 2(b), we show the ionization rates evaluated at $F = (2I_p)^{3/2} \times 0.05$ so that the reduced field \tilde{F} , defined as

$$\tilde{F} = \frac{F}{(2I_p)^{3/2}}, \quad (26)$$

equals 0.05 a.u. The reduced field \tilde{F} appears in the PPT rate as $\exp[-2/(3\tilde{F})]$ [see Eq. (C1)], and therefore, the PPT rate varies rapidly with \tilde{F} in the tunneling regime. The particular value of $\tilde{F} = 0.05$ a.u. was empirically proposed in [3] as a threshold for saturated ionization, beyond which atoms are completely ionized. The condition of $\tilde{F} = 0.05$ a.u. means that

the field strength is in the tunneling regime rather than in the over-barrier regime. For example, for $Z = 2$, $F = (2I_p)^{3/2} \times 0.05 = 0.12$ a.u. $< F_{\text{BS}} = 0.20$ a.u., and, for $Z = 10$, $F = (2I_p)^{3/2} \times 0.05 = 41$ a.u. $< F_{\text{BS}} = 54$ a.u. As shown in Fig. 2(b), the PPT-based fitting formula works well also at the reduced field of $\tilde{F} = 0.05$ a.u. Indeed, the deviations are sufficiently small in the entire range of Z , that is, $|\Gamma_{\text{fit}} - \Gamma|/\Gamma < 0.12$ for $Z \leq 12$ and $|\Gamma_{\text{fit}} - \Gamma|/\Gamma < 0.03$ for $Z > 12$. However, it should be noted that the quadratic function fits well only in the large Z above ~ 20 , that is, (i) $|\Gamma_{\text{fit}} - \Gamma|/\Gamma > 0.4$ for $Z < 10$, (ii) $0.4 > |\Gamma_{\text{fit}} - \Gamma|/\Gamma > 0.1$ for $10 \leq Z < 20$, and (iii) $|\Gamma_{\text{fit}} - \Gamma|/\Gamma < 0.1$ for $Z \geq 20$.

B. Ionization rates by perturbation theory

In Fig. 3, we compare the ionization rates Γ calculated using the MCTDHF method and the ionization rates Γ_{pert}^N [see Eq. (13)] calculated by perturbation theory. The numerical values of the expansion coefficients λ'_n given by Eq. (14) are shown in Appendix B 2. Our numerical approach for solving the equations of perturbation theory, described in Appendix B 2, limits the range of the scaled field strengths to $F' \geq 0.25$ a.u. for the orders of $n = 0$ and 1, and to $F' \geq 0.35$ a.u. for the orders of 2 and 3.

We can see in Figs. 3(a) and (b) that the rate $\Gamma_{\text{pert}}^{N=3}$ including the third-order corrections agrees well with the rate calculated with the MCTDHF method. For both $Z = 10$ and $Z = 18$, the relative deviations are as small as $|\Gamma_{\text{pert}}^{N=3} - \Gamma|/\Gamma < 0.07$ in the scaled field range of $F' \geq 0.4$ a.u. The values of $Z = 10$ and $Z = 18$ are selected to demonstrate the performance of perturbation theory for the large values of $Z \geq 10$, where the perturbation to the third order is enough to obtain ionization rates with a sufficiently small deviation from the reference MCTDHF rates. It can be seen in Figs. 3(a) and (b) that perturbation theory gives relatively accurate results for the ionization rate in both the tunneling and the OTB regimes (for $Z = 10$, $F'_{\text{BS}} = 0.43$ a.u., and for $Z = 18$, $F'_{\text{BS}} = 0.46$ a.u.). In the tunneling regime, where the ionization rate is exponentially sensitive to the variation in the ionization potential, it is necessary to include sufficiently large orders in perturbation theory so that an accurate value of the ground state energy is obtained. The results shown in Figs. 3(a) and (b) suggest that $N = 3$ is large enough to obtain ionization rates with a relative deviation from the MCTDHF rates below 7% both in the tunneling and the OTB regimes.

In Fig. 3(c), we show the ionization rates as a function of Z , evaluated at the scaled

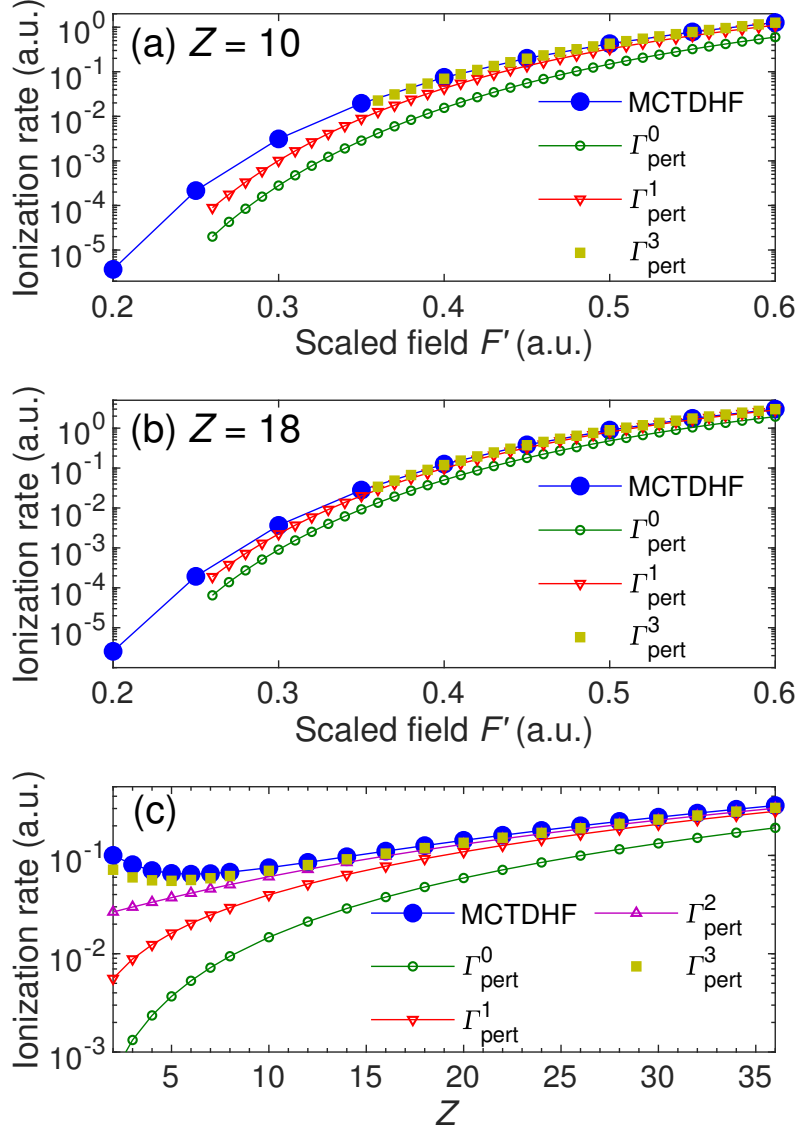


FIG. 3. Ionization rates for (a) $Z = 10$ and (b) $Z = 18$ obtained by the MCTDHF method (filled circles) and those obtained by perturbation theory as a function of the scaled field $F' = 8F/Z^3$. The perturbative rate Γ_{pert}^N contains corrections up to the order $1/Z^N$. In panel (c), we show the rates as a function of Z at a fixed value $F' = 0.4$ a.u. of the scaled field.

field of $F' = 0.4$ a.u. The deviation of the ionization rate calculated by the third order perturbation theory becomes smaller as Z increases, that is, $|\Gamma_{\text{pert}}^{N=3} - \Gamma|/\Gamma = 0.29$ for $Z = 2$, $|\Gamma_{\text{pert}}^{N=3} - \Gamma|/\Gamma = 0.09$ for $Z = 8$, and $|\Gamma_{\text{pert}}^{N=3} - \Gamma|/\Gamma < 0.07$ for $Z \geq 10$. However, the third-order rate $\Gamma_{\text{pert}}^{N=3}$ exhibits a minimum in the rate at $Z = 5$ in a similar manner as the MCTDHF rate exhibiting a minimum at $Z = 6$, as can be seen in the curves plotted with filled circles and filled squares in Fig. 3(c). This minimum in the ionization rate appearing

at a certain Z value can be explained by the asymptotic behavior of the PPT rate. At the fixed scaled field of $F' = 8F/Z^3 = 0.4$ a.u., the PPT rate increases as $\Gamma_{\text{PPT}} \propto Z^2$ for large Z ($Z > 30$). For the smaller values of $Z \leq 7$, where the ionization rate is in the tunneling regime, Γ_{PPT} decreases as Z increases because the reduced field $\tilde{F} \approx \frac{F'}{8} \left(1 - \frac{5}{4Z}\right)^{-\frac{3}{2}}$ decreases as Z increases. Therefore, in the intermediate range, there must be a minimum in the ionization rate, which is expected to appear approximately at the value of Z where $F' \approx F'_{\text{BS}}$. In the case of $F' = 0.4$ a.u., $F' < F'_{\text{BS}}$ when $Z \leq 7$.

C. Comparison of SAE approximation rates and MCTDHF rates

In Fig. 4, we show the comparison between the results obtained by the SAE approximation described in Sec. IID and those obtained by the MCTDHF method. The numerical values of the parameter ζ' are $\zeta' = 2.1325$ for $Z = 2$ and $\zeta' = 2.4489$ for $Z = 10$. For the polarization potential defined in Eq. (17), we employ the value $\eta = 4.8713$ for He ($Z = 2$), so that twice the polarizability α_{SAE} of the active electron equals the polarizability of He, $\alpha_{\text{He}} = 1.3832$ a.u. [63]. The numerical calculation of the SAE rates and the calculation of the SAE polarizability are described in Appendix E.

We can see in Fig. 4(a) that the SAE rate for He is larger than the MCTDHF rate by around 30% (31% for $F' = 0.4$ a.u. and 27% for $F' = 0.5$ a.u.). The agreement is not significantly improved when the polarization potential is included in the effective SAE potential, as defined in Eq. (18). On the other hand, the results obtained by the FC model defined in Eq. (21) agree very well with the MCTDHF results ($|\Gamma_{\text{FC}} - \Gamma|/\Gamma < 0.06$ for $F' \leq 0.4$ a.u.). Because the SAE model should give the correct ionization potential in its construction and the FC model, in which the correlated ground state is included in the wave function ansatz (21), should also give the correct ionization potential, the better agreement of the ionization rate given by the FC model cannot be attributed to the difference in the ionization potential. In addition, because the core polarization is not included in the FC model, the polarization of the He^+ core cannot be responsible for the difference between the SAE results and the FC results. The difference between the FC model and the SAE model can be ascribed to the exchange interaction between the ejected electron and the He^+ core that is not included in the SAE model but in the FC model. Indeed, the FC wave function (21) is symmetric with respect to the exchange of the two electron coordinates. Therefore,

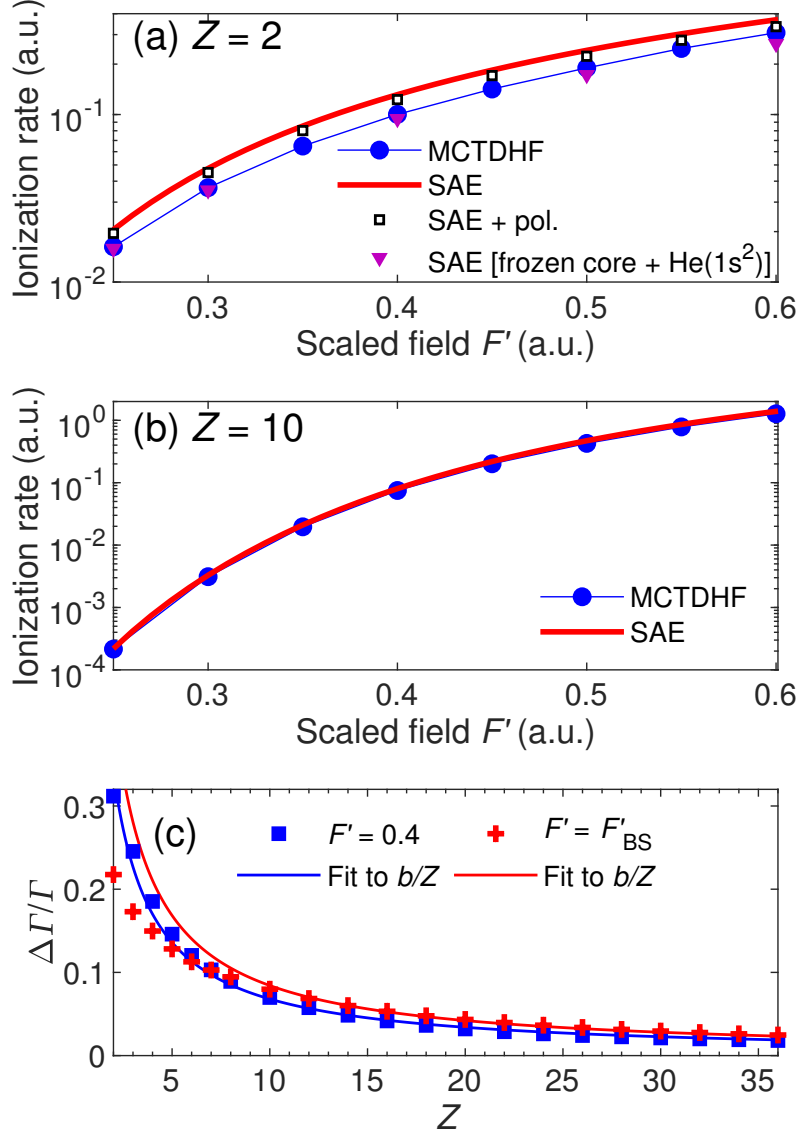


FIG. 4. Ionization rates $\Gamma = Z^2 \Gamma'/4$ as a function of F' for (a) He and (b) He-like Ne ($Z = 10$), calculated with the MCTDHF method and the SAE model, using potential V_1 [see Eq. (16)]. In (a) we additionally show the rates obtained with the SAE model including the polarization potential [see Eq. (18)], and the FC model including a correlated He ground state wave function [see Eq. (21)]. In (c), we show the relative deviation $\Delta\Gamma/\Gamma = (\Gamma_{\text{SAE}} - \Gamma)/\Gamma$ of the rate Γ_{SAE} obtained with the SAE approximation from the MCTDHF rate Γ as a function of Z , evaluated at $F' = 0.4$ a.u. and $F = F_{\text{BS}}$. Also shown are fits to the function b/Z , with $b(F' = 0.4) = 0.68$, and $b(F = F_{\text{BS}}) = 0.84$. In the case of $F = F_{\text{BS}}$, only $\Delta\Gamma/\Gamma$ values for $Z \geq 10$ were included in the fit.

the disagreement between the SAE rate and the MCTDHF rate is considered to originate from the exchange interaction. The overestimation of the ionization rate given by the SAE approximation can be ascribed to the increase in the ionization probability originating from the absence of the exchange interaction. The importance of the exchange interaction was reported before in the alignment dependence of the tunneling ionization rates in CO₂, O₂, and N₂ [36]. In order to further prove that the exchange interaction can affect the ionization process, we have included in Appendix F a discussion on two different frozen-core Hartree-Fock models, that is, one in which the exchange symmetry is fulfilled and the other in which no exchange symmetry is considered.

Figure 4(b), in which the MCTDHF rate and the SAE rate are compared for $Z = 10$, shows that the relative difference is less than 10% in the range of $0.25 \leq F' \leq 0.6$ a.u. In the case of $Z = 18$ (not shown in Fig. 4), the relative difference is smaller than 6% for $0.25 \leq F' \leq 0.6$ a.u., suggesting that the effect of the exchange interaction decreases as Z increases.

In order to quantify the effect of the exchange interaction, we define the relative deviation of the SAE rate from the MCTDHF rate as

$$\frac{\Delta\Gamma}{\Gamma} = \frac{\Gamma_{\text{SAE}} - \Gamma}{\Gamma}, \quad (27)$$

where Γ denotes the ionization rate calculated by the MCTDHF method, and show $\Delta\Gamma/\Gamma$ as a function of Z in Fig. 4(c). We evaluate the relative deviation at two different field strengths, $F' = 0.4$ a.u., and $F = F_{\text{BS}}$. In both cases, the relative deviation $\Delta\Gamma/\Gamma$ decreases approximately as $1/Z$ as Z increases, and the decrease proportional to $1/Z$ is shown clearly by the best fit curves having the form of b/Z with a constant factor of b . The deviation of the SAE rate from the MCTDHF rate caused by the exchange interaction is approximately 30% in He, and the deviation decreases as $1/Z$ to about 2% in He-like Kr.

IV. SUMMARY AND CONCLUSIONS

We have performed an investigation of the static-field ionization rates of He-like ions for the nuclear charge numbers Z up to $Z = 36$, in both the tunneling and OTB regimes. We have made two major findings. The first is that both the PPT-based fitting formula by Tong and Lin [38] [see Eq. (22) and Table I] and the third-order perturbation theory in $1/Z$

[see Eq. (13)] give small deviations from the rates calculated by the MCTDHF method. In the case of the PPT-based fitting formula, the relative deviation from the reference rates obtained by the MCTDHF method is about 10% when $Z > 2$ and $F \leq 0.075Z^3$ a.u., corresponding to scaled fields $F' \leq 0.6$ a.u. In the case of the ionization rates calculated with third-order perturbation theory, the relative deviation from the MCTDHF rates is 7% for $Z \geq 10$. In practice, the PPT-based fitting formula with the parameter α whose values are given in Table I provides reasonably good estimates of the ionization rate and will help researchers estimate the ion yields in the intensity measurement scheme proposed in [3, 4].

The second finding is that the exchange interaction in the tunneling and OTB barrier ionization reduces the ionization rate by an amount proportional to $1/Z$, ranging from a reduction of 30% for He ($Z = 2$) to about 2% for He-like Kr ($Z = 36$). This demonstrates the importance of the exchange interaction in the strong-field ionization of He-like ions, and shows how the relative strength of the exchange interaction decreases as the nuclear charge number Z increases.

ACKNOWLEDGMENTS

This research was supported by JSPS KAKENHI grants no. JP18K05024 and no. JP15H05696, a JSPS Invitational Fellowship for Research in Japan (no. S18108), and a travel grant from the Czech Academy of Sciences (no. VAJVA-19-04). M. F. C. acknowledges the project Advanced research using high intensity laser produced photons and particles (CZ.02.1.01/0.0/0.0/ 16_019/0000789) from European Regional Development Fund (ADONIS), the Spanish Ministry MINECO (National Plan 15 Grant: FISICATEAMO No. FIS2016-79508-P, SEVERO OCHOA No. SEV-2015-0522, FPI), European Social Fund, Fundació Cellex, Generalitat de Catalunya (AGAUR Grant No. 2017 SGR 1341 and CERCA/Program), ERC AdG NOQIA, and the National Science Centre, Poland-Symfonia Grant No. 2016/20/W/ST4/ 00314.

Appendix A: Numerical implementation of the MCTDHF method

The numerical method used for the solution of the MCTDHF equations of motion is the same as that presented in [51, 55]. We describe the essential points below. The MCTDHF

rates are obtained with $M = 10$ spatial orbitals for He. The orbitals can initially (at $t' = 0$) be characterized as $4s3p3p'$. For $Z > 2$, we employ $M = 6$ ($3s3p$). The spatial orbitals $\phi'_j(\mathbf{r}', t')$ are written as

$$\phi'_j(\mathbf{r}', \omega, t') = \sum_{\ell=0}^{\ell_{\max}} \frac{f_{\ell j}(r', t')}{r'} Y_{\ell, m_j}(\theta', \varphi'), \quad (\text{A1})$$

where $Y_{\ell, m}(\theta', \varphi')$ are spherical harmonics and $\ell_{\max} = 10$. The magnetic quantum number m_j is fixed for each orbital. The radial functions $f_{\ell j}(r')$ are discretized on a non-uniform mesh with $r' < 60$ a.u. and an asymptotic mesh width $\Delta r' = 0.2$ a.u. at large $r' > 5$ a.u. The grid points at smaller r' are distributed such that the error in the ground state energy $\varepsilon_0(\text{He}^+)$ of He^+ is minimized. We obtain $\varepsilon_0(\text{He}^+) = -2 + 2 \times 10^{-9}$ a.u. For the ground state of He (two electrons), we obtain with $M = 10$ spatial orbitals a value of $\varepsilon_0(\text{He}) = -2.8990$ a.u., which is 0.2% larger than the exact, non-relativistic ground state energy $\varepsilon_0^{\text{exact}}(\text{He}) \approx -2.9037$ a.u. [64].

The time evolution is calculated by a predictor-corrector method similar to that presented in [65], with a time step of $\delta t' = 5 \times 10^{-3}$ a.u. Further details can be found in Appendix E of [55].

Appendix B: Perturbation theory

1. Equations for χ'_n and ϵ'_n

The equations for perturbation theory up to order three in $1/Z$ are given as

$$\chi'_0(\mathbf{r}'_1, \mathbf{r}'_2) = \xi'_0(\mathbf{r}'_1) \xi'_0(\mathbf{r}'_2), \quad (\text{B1})$$

$$h'_0 \xi'_0(\mathbf{r}') = \frac{\epsilon'_0}{2} \xi'_0(\mathbf{r}'), \quad (\text{B2})$$

where h'_0 is the complex-rotated single-electron Hamiltonian for H-like He,

$$h'_0 = -\frac{e^{-2i\Theta}}{2} \frac{\partial^2}{\partial \mathbf{r}'^2} - \frac{2e^{-i\Theta}}{r'} + e^{i\Theta} F' z', \quad (\text{B3})$$

$$\epsilon'_1 = \left(\chi'_0 \left| \frac{2e^{-i\Theta}}{r'_{12}} \right| \chi'_0 \right), \quad (\text{B4})$$

$$\begin{aligned} & \left[\sum_{i=1,2} h'_0(e^{i\Theta} \mathbf{r}'_i) - \epsilon'_0 \right] \chi'_1(\mathbf{r}'_1, \mathbf{r}'_2) \\ &= \left(\epsilon'_1 - \frac{2e^{-i\Theta}}{r'_{12}} \right) \chi'_0(\mathbf{r}'_1, \mathbf{r}'_2), \end{aligned} \quad (\text{B5})$$

$$\epsilon'_2 = \left(\chi'_0 \left| \frac{2e^{-i\Theta}}{r'_{12}} \right| \chi'_1 \right), \quad (\text{B6})$$

$$\begin{aligned} & \left[\sum_{i=1,2} h'_0(e^{i\Theta} \mathbf{r}'_i) - \epsilon'_0 \right] \chi'_2(\mathbf{r}'_1, \mathbf{r}'_2) \\ &= \left(\epsilon'_1 - \frac{2e^{-i\Theta}}{r'_{12}} \right) \chi'_1(\mathbf{r}'_1, \mathbf{r}'_2) + \epsilon'_2 \chi'_0(\mathbf{r}'_1, \mathbf{r}'_2), \end{aligned} \quad (\text{B7})$$

and finally

$$\epsilon'_3 = \left(\chi'_0 \left| \frac{2e^{-i\Theta}}{r'_{12}} - \epsilon'_1 \right| \chi'_2 \right). \quad (\text{B8})$$

The inner product $(\chi|\tilde{\chi})$ between two complex-rotated wave functions χ and $\tilde{\chi}$ is denoted by round brackets, and is defined as

$$(\chi|\tilde{\chi}) = \int d^3r'_1 d^3r'_2 \chi(\mathbf{r}'_1, \mathbf{r}'_2) \tilde{\chi}(\mathbf{r}'_1, \mathbf{r}'_2), \quad (\text{B9})$$

without the complex conjugate on the left-hand wave function χ [66, 67].

To ensure that the wave function is consistently normalized to 1 at each order of $1/Z$, we should normalize χ'_0 as $(\chi'_0|\chi'_0) = 1$. We also have to project out the χ'_0 -component in χ'_1 such that $(\chi'_0|\chi'_1) = 0$ is satisfied after solving Eq. (B5). Similarly, after solving Eq. (B7), we have to adjust χ'_2 according to $\chi'_2 \rightarrow \chi'_2 - \kappa \chi'_0$ with $\kappa = (\chi'_0|\chi'_2) + (\chi'_1|\chi'_1)/2$, such that $(\chi'_0|\chi'_2) = -(\chi'_1|\chi'_1)/2$ is satisfied.

2. Numerical values of λ'_n

Equation (B2) is a single-particle equation, and is solved by expanding $\xi'_0(\mathbf{r}')$ in the same way as shown in Eq. (A1), using a radial grid with $\Delta r = 3 \times 10^{-4}$ a.u., $\ell_{\max} = 5$, and $m = 0$. This approach is limited to scaled fields F' larger than 0.25 a.u. To obtain ξ'_0 and $\epsilon'_{0,1}$ at smaller values of F' requires more sophisticated methods, such as those in which multiple-precision arithmetic is employed (see Appendix B of Ref. [29]). We solve the Eqs. (B5) and (B7) by expanding the n th-order wave function χ'_n as

$$\begin{aligned} \chi'_n(\mathbf{r}'_1, \mathbf{r}'_2) &= \sum_{\ell, \ell'=0}^{\ell_{\max}} \sum_{m=-m_{\max}}^{m_{\max}} \frac{C_{\ell\ell'm}(r'_1, r'_2)}{r'_1 r'_2} \\ &\quad \times Y_{\ell, -m}(\theta'_1, \varphi'_1) Y_{\ell', m}(\theta'_2, \varphi'_2), \end{aligned} \quad (\text{B10})$$

and employ a grid with $\Delta r' = 0.2$ a.u., $r' < 30$ a.u., $m_{\max} = 2$, and $\ell_{\max} = 5$. We define $Y_{\ell, m} = 0$ when $|m| > \ell$. The electron-electron interaction term $1/r'_{12}$ is dealt with by the

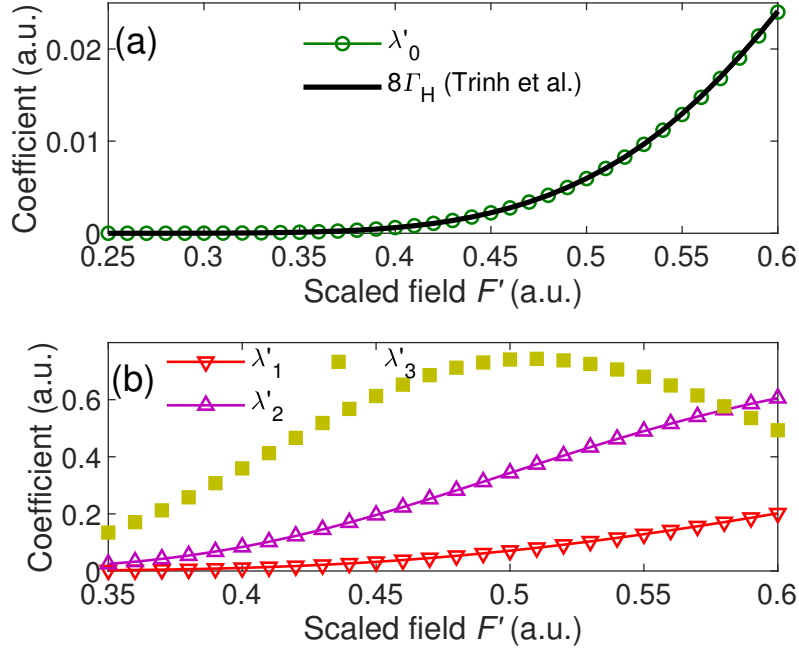


FIG. 5. (a) Zeroth-order expansion coefficient λ'_0 and eight times the ionization rate Γ_H of hydrogen, taken from Trinh et al. [29]. (b) Expansion coefficients λ'_n for the orders $n = 1, 2$, and 3.

standard expansion in spherical harmonics [68]. Note that both χ'_1 and χ'_2 are correlated two-electron wave functions, and Eqs. (B5) and (B7) are therefore considerably more difficult to be solved than Eq. (B2). For $\epsilon_{2,3}$, our approach is limited to scaled fields $F' \geq 0.35$ a.u.

In Fig. 5, we show the expansion coefficients λ'_n ($n = 0, 1, \dots, 3$) which are used in Eq. (13) for the evaluation of the ionization rate by perturbation theory. According to Eq. (9), we have $\lambda'_0(F') = 8\Gamma_H(F'/8)$, where Γ_H is the ionization rate for H, and we therefore show also Γ_H (taken from [29]) in Fig. 5(a) for comparison. The agreement between our results for λ'_0 and the ionization rates for H presented in [27–29] is better than 1% for $F \geq 0.3$ a.u.

Appendix C: PPT formula

The PPT formula employed in this paper reads [4, 9, 11]

$$\Gamma_{\text{PPT}} = 2C_\nu^2 I_p \tilde{F}^{1-2\nu} \exp\left(-\frac{2}{3\tilde{F}}\right), \quad (\text{C1})$$

where

$$\nu = \frac{Z-1}{\sqrt{2I_p}} \quad (\text{C2})$$

is the effective principal quantum number defined in terms of the ionization potential I_p , the reduced field \tilde{F} is defined in Eq. (26), and

$$C_\nu^2 = \frac{2^{4\nu-1}}{\nu\Gamma(\nu+1)\Gamma(\nu)}. \quad (\text{C3})$$

Note the additional factor of 2 in the expression (C1) which accounts for the contribution of two electrons.

In order to have a consistent definition of the ionization potential I_p for all values of Z , we employ the expansion in inverse powers of Z of the ground state energy $\varepsilon_0(Z)$ of a He-like ion given in [69],

$$\varepsilon_0(Z) = Z^2 \sum_{n=0}^{25} \frac{a_n}{Z^n}. \quad (\text{C4})$$

The coefficients a_n in Eq. (C4) are taken from table XII in [69]. The first two coefficients $a_0 = -1$ and $a_1 = 5/8$ are known analytically, but a_n for $n > 1$ have to be calculated numerically. The ionization potential is calculated as

$$I_p(Z) = -\frac{Z^2}{2} - \varepsilon_0(Z). \quad (\text{C5})$$

Compared to the exact nonrelativistic ground state energy of He, $\varepsilon_0^{\text{exact}}(Z=2) \approx -2.9037$ a.u. [64], the expression (C4) gives $\varepsilon_0(2) - \varepsilon_0^{\text{exact}}(2) \approx 10^{-7}$ a.u., while for $Z=10$ we have $\varepsilon_0^{\text{exact}}(Z=10) \approx -93.9068$ a.u. [64] and $\varepsilon_0(10) - \varepsilon_0^{\text{exact}}(10) \approx 5 \times 10^{-8}$. This shows that the formula (C4) has a relative accuracy of $[\varepsilon_0(Z) - \varepsilon_0^{\text{exact}}(Z)]/|\varepsilon_0^{\text{exact}}(Z)| < 4 \times 10^{-8}$. The experimental ionization potentials are $I_p^{\text{exp}}(Z=2) \approx 0.9036$ a.u. and $I_p^{\text{exp}}(Z=10) \approx 43.9451$ a.u. [70]; the differences $I_p^{\text{exp}}(2) - I_p(2) \approx -1.5 \times 10^{-4}$ a.u. and $I_p^{\text{exp}}(10) - I_p(10) \approx 0.038$ a.u. can be attributed to corrections to the energy levels originating from the finite nuclear mass and relativistic effects.

Appendix D: Numerical values of ionization rates for He

In this Appendix, we list in Table II the values of the ionization rates Γ obtained in the present work by the MCTDHF method, together with the ionization rate Γ_{SGB} calculated by Scrinzi, Geissler, and Brabec [31] and the ionization rate Γ_{PABT} calculated by Parker, Armstrong, Boca, and Taylor [37]. The relative deviations from the MCTDHF rates are $|\Gamma_{\text{SGB}} - \Gamma|/\Gamma_{\text{SGB}} < 0.08$ and $|\Gamma_{\text{PABT}} - \Gamma|/\Gamma_{\text{PABT}} < 0.04$ in the range of F shown in Table II.

TABLE II. Static-field ionization rates Γ of He obtained by different approaches.

$F/\text{a.u.}$	$\Gamma/\text{a.u. (MCTDHF)}$	$\Gamma_{\text{SGB}}/\text{a.u. [31]}$	$\Gamma_{\text{PABT}}/\text{a.u. [37]}$
0.10	2.91×10^{-6}	2.88×10^{-6}	2.9391×10^{-6}
0.15	4.32×10^{-4}	4.23×10^{-4}	4.2913×10^{-4}
0.20	4.49×10^{-3}	4.31×10^{-3}	4.3347×10^{-3}
0.25	1.62×10^{-2}	1.57×10^{-2}	1.5793×10^{-2}
0.30	3.66×10^{-2}	3.56×10^{-2}	3.5857×10^{-2}
0.35	6.48×10^{-2}	6.33×10^{-2}	
0.40	1.00×10^{-2}	9.77×10^{-2}	
0.45	1.42×10^{-1}	1.38×10^{-1}	
0.50	1.90×10^{-1}	1.83×10^{-1}	
0.55	2.48×10^{-1}	2.33×10^{-1}	
0.60	3.08×10^{-1}	2.87×10^{-1}	

Appendix E: Numerical implementation of the single-active electron approximation

We solve the eigenvalue equation (19) for the SAE rate by expanding the wave function in the same manner as shown in Eq. (A1), but using a smaller $\Delta r' = 3 \times 10^{-4}$ a.u. for the radial grid, $m = 0$, and $\ell_{\text{max}} = 5$.

In the frozen core model defined in Eq. (21), we adopt the expansion (A1) for $\phi(\mathbf{r}, t)$, and we employ a MCTDHF wave function ($M = 10$) as defined in Eq. (8) for $\Psi_0^{\text{He}}(\mathbf{r}_1, \mathbf{r}_2)$.

Within the SAE approximation, the polarizability α_{SAE} is calculated as

$$\alpha_{\text{SAE}} = -2\langle\psi_{\text{SAE}}^0|z|\psi_{\text{SAE}}^1\rangle, \quad (\text{E1})$$

where ψ_{SAE}^0 is the ground state of the field-free SAE Hamiltonian $H_{\text{SAE}}(F = 0)$,

$$H_{\text{SAE}}(F = 0)\psi_{\text{SAE}}^0 = \varepsilon_0\psi_{\text{SAE}}^0, \quad (\text{E2})$$

and ψ_{SAE}^1 solves

$$[H_{\text{SAE}}(F = 0) - \varepsilon_0]\psi_{\text{SAE}}^1 = -\left[z + \frac{V_{\text{pol}}(\mathbf{r})}{F}\right]\psi_{\text{SAE}}^0. \quad (\text{E3})$$

The parameter η in Eq. (17) is adjusted so that

$$2\alpha_{\text{SAE}} = \alpha_{\text{He}}, \quad (\text{E4})$$

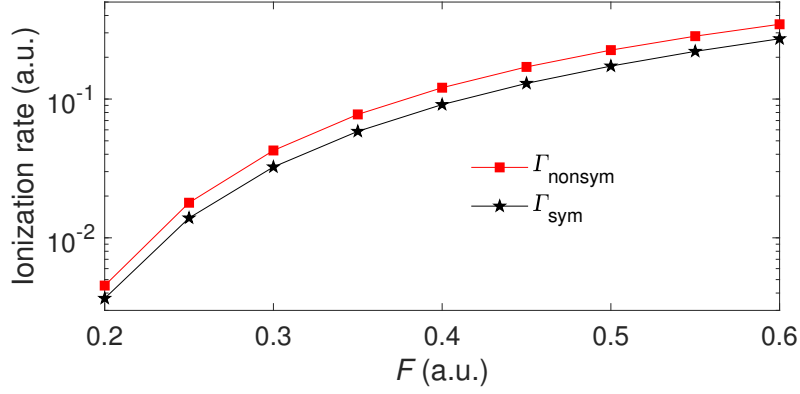


FIG. 6. Static-field ionization rate Γ_{sym} of He calculated by the Hartree-Fock model defined in Eq. (F1) where exchange symmetry is fulfilled and the ionization rate Γ_{nonsym} calculated by the Hartree-Fock model defined in Eq. (F2) where no exchange symmetry is considered.

where $\alpha_{\text{He}} = 1.3832$ a.u. is the polarizability of He [63].

Appendix F: Frozen-core Hartree-Fock model with and without symmetrization

In order to corroborate that the exchange interaction can influence the ionization rate, we consider two different wave function models of Hartree-Fock type for He. In the first, the two-electron wave function is written as

$$\Psi_{\text{HF(sym)}}(\mathbf{r}_1, \mathbf{r}_2, t) = \frac{1}{\sqrt{2}} [\psi_{1s}^{\text{HF}}(\mathbf{r}_1)\phi(\mathbf{r}_2, t) + \phi(\mathbf{r}_1, t)\psi_{1s}^{\text{HF}}(\mathbf{r}_2)], \quad (\text{F1})$$

where $\psi_{1s}^{\text{HF}}(\mathbf{r})$ is the Hartree-Fock ground state of the 1s orbital of He, and $\phi(\mathbf{r}, t)$ is a time-dependent wave function describing the ejected electron with initial condition $\phi(\mathbf{r}, t=0) = \psi_{1s}^{\text{HF}}(\mathbf{r})/\sqrt{2}$. The wave function defined in Eq. (F1) has the correct symmetry with respect to the exchange of the electron coordinates.

In the second model, we take a wave function of the form

$$\Psi_{\text{HF(nonsym)}}(\mathbf{r}_1, \mathbf{r}_2, t) = \psi_{1s}^{\text{HF}}(\mathbf{r}_1)\phi(\mathbf{r}_2, t), \quad (\text{F2})$$

which is not symmetric with respect to the exchange of the two electron coordinates. The initial condition for $\phi(\mathbf{r}, t)$ in Eq. (F2) is $\phi(\mathbf{r}, t=0) = \psi_{1s}^{\text{HF}}(\mathbf{r})$.

Both models (F1) and (F2) have the same ground state, that is, the Hartree-Fock ground state, $\Psi_{\text{HF(sym)}}^0(\mathbf{r}_1, \mathbf{r}_2) = \Psi_{\text{HF(nonsym)}}^0(\mathbf{r}_1, \mathbf{r}_2) = \psi_{1s}^{\text{HF}}(\mathbf{r}_1)\psi_{1s}^{\text{HF}}(\mathbf{r}_2)$, and therefore, the same

ionization potential. The only difference is the absence of exchange symmetry in Eq. (F2). Because the ionization potential of the models (F1) and (F2) is too large, $I_p^{\text{HF}} = 0.9169$ a.u. compared to the accurate value of $I_p = 0.9037$ a.u. given by Eq. (C5), the resulting ionization rates are not quantitatively accurate, but the two models can be used to demonstrate the effect of the exchange interaction during the ionization.

The ionization rates for He obtained by the models (F1) and (F2) are shown in Fig. 6. The numerical calculation was performed in the same way as described in Appendix E. In the non-symmetric model Eq. (F2), the ionization rate is multiplied with a factor of 2 to account for the indistinguishability of the electrons.

We can see in Fig. 6 that the ionization rate Γ_{nonsym} for the non-symmetric model is larger than the ionization rate Γ_{sym} for the symmetric model. The relative difference given by $(\Gamma_{\text{nonsym}} - \Gamma_{\text{sym}})/\Gamma_{\text{sym}}$ is 0.32 at $F = 0.4$ a.u. and that at $F = 0.5$ a.u. is 0.30. These values of the relative difference are similar to the values of the relative difference $(\Gamma_{\text{SAE}} - \Gamma)/\Gamma$ between the rate Γ_{SAE} obtained by the SAE approximation and the rate Γ obtained by the MCTDHF method, where we obtain $(\Gamma_{\text{SAE}} - \Gamma)/\Gamma = 0.31$ at $F = 0.4$ a.u. and $(\Gamma_{\text{SAE}} - \Gamma)/\Gamma = 0.27$ at $F = 0.5$ a.u., as shown in Fig. 4(a) in Sec. III C. Because the only difference between the two wave functions (F1) and (F2) is the exchange symmetry, we conclude that inclusion of the exchange symmetry reduces the ionization rate by approximately 30% also in the case of Hartree-Fock type wave functions.

-
- [1] H. G. Hetzheim and C. H. Keitel, “Ionization dynamics versus laser intensity in laser-driven multiply charged ions,” *Phys. Rev. Lett.* **102**, 083003 (2009).
 - [2] H. Bauke, H. G. Hetzheim, G. R. Mocken, M. Ruf, and C. H. Keitel, “Relativistic ionization characteristics of laser-driven hydrogenlike ions,” *Phys. Rev. A* **83**, 063414 (2011).
 - [3] M. F. Ciappina, S. V. Popruzhenko, S. V. Bulanov, T. Ditmire, G. Korn, and S. Weber, “Progress toward atomic diagnostics of ultrahigh laser intensities,” *Phys. Rev. A* **99**, 043405 (2019).
 - [4] M. F. Ciappina and S. V. Popruzhenko, “Diagnostics of ultra-intense laser pulses using tunneling ionization,” *Laser Phys. Lett.* **17**, 025301 (2020).
 - [5] M. F. Ciappina, S. Bulanov, T. Ditmire, G. Korn, and S. Weber, “Towards laser intensity

- calibration using high-field ionization,” in *Progress in Ultrafast Intense Laser Science*, Topics in Applied Physics 136, Vol. XV, edited by K. Yamanouchi and D. Charalambidis (Springer Nature, Switzerland, 2020) Chap. 8, pp. 149–176.
- [6] B. Rus, P. Bakule, D. Kramer, J. Naylon, J. Thoma, J. T. Green, R. Antipenkov, M. Fibrich, J. Novák, F. Batysta, T. Mazanec, M. A. Drouin, K. Kasl, R. Baše, D. Peceli, L. Koubíková, P. Trojek, R. Boge, J. C. Lagron, Š. Vyhlídka, J. Weiss, J. Cupal, J. Hřebíček, P. Hříbek, M. Ďurák, J. Polan, M. Košelja, G. Korn, M. Horáček, J. Horáček, B. Himmel, T. Havlíček, A. Honsa, P. Korouš, M. Laub, C. Haefner, A. Bayramian, T. Spinka, C. Marshall, G. Johnson, S. Telford, J. Horner, B. Deri, T. Metzger, M. Schultze, P. Mason, K. Ertel, A. Lintern, J. Greenhalgh, C. Edwards, C. Hernandez-Gomez, J. Collier, T. Ditmire, E. Gaul, M. Martinez, C. Frederickson, D. Hammond, C. Malato, W. White, and J. Houžvička, “ELI-Beamlines: development of next generation short-pulse laser systems,” in *Research Using Extreme Light: Entering New Frontiers with Petawatt-Class Lasers II*, Vol. 9515, edited by G. Korn and L. O. Silva, International Society for Optics and Photonics (SPIE, 2015) pp. 34 – 44.
- [7] Z. Guo, L. Yu, J. Wang, C. Wang, Y. Liu, Z. Gan, W. Li, Y. Leng, X. Liang, and R. Li, “Improvement of the focusing ability by double deformable mirrors for 10-PW-level Ti: sapphire chirped pulse amplification laser system,” *Opt. Express* **26**, 26776 (2018).
- [8] B. M. Smirnov and M. I. Chibisov, “The breaking up of atomic particles by an electric field and by electron collisions,” *Zh. Eksp. Teor. Fiz.* **49**, 841 (1965), [*Sov. Phys. JETP* **22**, 585 (1966) (Engl. transl.)].
- [9] A. M. Perelomov, V. S. Popov, and M. V. Terentev, “Ionization of atoms in an alternating electric field,” *Zh. Eksp. Teor. Fiz.* **50**, 1393 (1966), [*Sov. Phys. JETP* **23** 924 (1966) (Engl. transl.)].
- [10] V. S. Popov, “Tunnel and multiphoton ionization of atoms and ions in a strong laser field (Keldysh theory),” *Physics-Uspekhi* **47**, 855 (2004).
- [11] S. V. Popruzhenko, “Keldysh theory of strong field ionization: history, applications, difficulties and perspectives,” *J. Phys. B* **47**, 204001 (2014).
- [12] M. V. Ammosov, N. B. Delone, and V. P. Krainov, “Tunnel ionization of complex atoms and of atomic ions in an alternating electromagnetic field,” *Zh. Eksp. Teor. Fiz.* **91**, 2008 (1986), [*Sov. Phys. JETP* **64** 1191 (1986) (Engl. transl.)].

- [13] X. M. Tong, Z. X. Zhao, and C. D. Lin, “Theory of molecular tunneling ionization,” *Phys. Rev. A* **66**, 033402 (2002).
- [14] T. K. Kjeldsen and L. B. Madsen, “Strong-field ionization of N_2 : length and velocity gauge strong-field approximation and tunnelling theory,” *J. Phys. B* **37**, 2033 (2004).
- [15] S.-F. Zhao, J. Xu, C. Jin, A.-T. Le, and C. D. Lin, “Effect of orbital symmetry on the orientation dependence of strong field tunnelling ionization of nonlinear polyatomic molecules,” *J. Phys. B* **44**, 035601 (2011).
- [16] A. S. Kornev and B. A. Zon, “Tunneling ionization of vibrationally excited nitrogen molecules,” *Phys. Rev. A* **92**, 033420 (2015).
- [17] A. S. Kornev, V. E. Chernov, and B. A. Zon, “Laser-induced deformation of triatomic molecules: Influence on tunnel ionization,” *Phys. Rev. A* **96**, 053408 (2017).
- [18] D. Fisher, Y. Maron, and L. P. Pitaevskii, “Ionization of many-electron atoms by a quasistatic electric field,” *Phys. Rev. A* **58**, 2214 (1998).
- [19] T. Brabec, M. Côté, P. Boulanger, and L. Ramunno, “Theory of tunnel ionization in complex systems,” *Phys. Rev. Lett.* **95**, 073001 (2005).
- [20] O. I. Tolstikhin, T. Morishita, and L. B. Madsen, “Theory of tunneling ionization of molecules: Weak-field asymptotics including dipole effects,” *Phys. Rev. A* **84**, 053423 (2011).
- [21] O. I. Tolstikhin, L. B. Madsen, and T. Morishita, “Weak-field asymptotic theory of tunneling ionization in many-electron atomic and molecular systems,” *Phys. Rev. A* **89**, 013421 (2014).
- [22] I. Y. Tolstikhina, T. Morishita, and O. I. Tolstikhin, “Application of the many-electron weak-field asymptotic theory of tunneling ionization to atoms,” *Phys. Rev. A* **90**, 053413 (2014).
- [23] V. H. Trinh, O. I. Tolstikhin, and T. Morishita, “Weak-field asymptotic theory of tunneling ionization: benchmark analytical results for two-electron atoms,” *J. Phys. B* **48**, 061003 (2015).
- [24] V. H. Trinh, O. I. Tolstikhin, and T. Morishita, “First-order correction terms in the weak-field asymptotic theory of tunneling ionization in many-electron systems,” *J. Phys. B* **49**, 195603 (2016).
- [25] L. Yue, S. Bauch, and L. B. Madsen, “Electron correlation in tunneling ionization of diatomic molecules: An application of the many-electron weak-field asymptotic theory with a generalized-active-space partition scheme,” *Phys. Rev. A* **96**, 043408 (2017).
- [26] A. I. Dnestryan, O. I. Tolstikhin, F. Jensen, and L. B. Madsen, “Torsional effects in strong-

- field ionization of molecules,” *Phys. Rev. Research* **1**, 023018 (2019).
- [27] C. A. Nicolaides and S. I. Themelis, “Theory of the resonances of the LoSurdo-Stark effect,” *Phys. Rev. A* **45**, 349 (1992).
 - [28] H. O. Karlsson and O. Goscinski, “Perturbed hydrogenic manifolds studied by the recursive residue generation method,” *J. Phys. B* **25**, 5015 (1992).
 - [29] V. H. Trinh, O. I. Tolstikhin, L. B. Madsen, and T. Morishita, “First-order correction terms in the weak-field asymptotic theory of tunneling ionization,” *Phys. Rev. A* **87**, 043426 (2013).
 - [30] C. A. Nicolaides and S. I. Themelis, “Theory and computation of electric-field-induced tunneling rates of polyelectronic atomic states,” *Phys. Rev. A* **47**, 3122 (1993).
 - [31] A. Scrinzi, M. Geissler, and T. Brabec, “Ionization above the Coulomb barrier,” *Phys. Rev. Lett.* **83**, 706 (1999).
 - [32] A. Scrinzi, “Ionization of multielectron atoms by strong static electric fields,” *Phys. Rev. A* **61**, 041402(R) (2000).
 - [33] A. Saenz, “Enhanced ionization of molecular hydrogen in very strong fields,” *Phys. Rev. A* **61**, 051402(R) (2000).
 - [34] T.-C. Jagau, “Investigating tunnel and above-barrier ionization using complex-scaled coupled-cluster theory,” *J. Chem. Phys.* **145**, 204115 (2016).
 - [35] V. P. Majety and A. Scrinzi, “Static field ionization rates for multi-electron atoms and small molecules,” *J. Phys. B* **48**, 245603 (2015).
 - [36] V. P. Majety and A. Scrinzi, “Dynamic exchange in the strong field ionization of molecules,” *Phys. Rev. Lett.* **115**, 103002 (2015).
 - [37] J. S. Parker, G. S. J. Armstrong, M. Boca, and K. T. Taylor, “From the UV to the static-field limit: rates and scaling laws of intense-field ionization of helium,” *J. Phys. B* **42**, 134011 (2009).
 - [38] X. M. Tong and C. D. Lin, “Empirical formula for static field ionization rates of atoms and molecules by lasers in the barrier-suppression regime,” *J. Phys. B* **38**, 2593 (2005).
 - [39] J. Zanghellini, M. Kitzler, C. Fabian, T. Brabec, and A. Scrinzi, “An MCTDHF approach to multielectron dynamics in laser fields,” *Laser Phys.* **13**, 1064 (2003).
 - [40] T. Kato and H. Kono, “Time-dependent multiconfiguration theory for electronic dynamics of molecules in an intense laser field,” *Chem. Phys. Lett.* **392**, 533 (2004).
 - [41] N. Milosevic, V. P. Krainov, and T. Brabec, “Semiclassical Dirac theory of tunnel ionization,”

- Phys. Rev. Lett. **89**, 193001 (2002).
- [42] L. V. Keldysh, “Ionization in the field of a strong electromagnetic wave,” *Zh. Éksp. Teor. Fiz.* **47**, 1945 (1964), [*Sov. Phys. JETP* **20**, 1307 (1965)].
 - [43] C. W. Scherr and R. E. Knight, “Two-electron atoms III. A sixth-order perturbation study of the 1^1S ground state,” *Rev. Mod. Phys.* **35**, 436 (1963).
 - [44] D. Hochstuhl, C. M. Hinz, and M. Bonitz, “Time-dependent multiconfiguration methods for the numerical simulation of photoionization processes of many-electron atoms,” *Eur. Phys. J. Spec. Top.* **223**, 177 (2014).
 - [45] K. Ishikawa and T. Sato, “A review on ab initio approaches for multielectron dynamics,” *IEEE J. Sel. Topics Quantum Electron.* **21**, 1 (2015).
 - [46] E. Lötstedt, T. Kato, and K. Yamanouchi, “Multiconfiguration methods for time-dependent many-electron dynamics,” in *Progress in Ultrafast Intense Laser Science XIII*, Springer Series in Chemical Physics, Vol. 116, edited by K. Yamanouchi, W. T. Hill III, and G. G. Paulus (Springer International Publishing, Switzerland, 2017) pp. 15–40.
 - [47] T. Sato, Y. Orimo, T. Teramura, O. Tugs, and K. L. Ishikawa, “Time-dependent complete-active-space self-consistent-field method for ultrafast intense laser science,” in *Progress in Ultrafast Intense Laser Science XIV*, Springer Series in Chemical Physics, Vol. 118, edited by K. Yamanouchi, P. Martin, M. Sentis, L. Ruxin, and D. Normand (Springer International Publishing, 2018) pp. 143–171.
 - [48] D. Hochstuhl and M. Bonitz, “Two-photon ionization of helium studied with the multiconfigurational time-dependent Hartree-Fock method,” *J. Chem. Phys.* **134**, 084106 (2011).
 - [49] T. Sato, K. L. Ishikawa, I. Březinová, F. Lackner, S. Nagele, and J. Burgdörfer, “Time-dependent complete-active-space self-consistent-field method for atoms: Application to high-order harmonic generation,” *Phys. Rev. A* **94**, 023405 (2016).
 - [50] Y. Orimo, T. Sato, A. Scrinzi, and K. L. Ishikawa, “Implementation of the infinite-range exterior complex scaling to the time-dependent complete-active-space self-consistent-field method,” *Phys. Rev. A* **97**, 023423 (2018).
 - [51] E. Lötstedt, T. Szidarovszky, F. H. M. Faisal, T. Kato, and K. Yamanouchi, “Excited-state populations in the multiconfiguration time-dependent Hartree-Fock method,” *J. Phys. B* **53**, 105601 (2020).
 - [52] J. Zhang and P. Lambropoulos, “Non-perturbative time-dependent theory and ATI in two

- electron atoms,” J. Phys. B **28**, L101 (1995).
- [53] E. S. Smyth, J. S. Parker, and K. Taylor, “Numerical integration of the time-dependent schrödinger equation for laser-driven helium,” Comput. Phys. Commun. **114**, 1 (1998).
 - [54] S. Laulan and H. Bachau, “Correlation effects in two-photon single and double ionization of helium,” Phys. Rev. A **68**, 013409 (2003).
 - [55] E. Lötstedt, T. Kato, and K. Yamanouchi, “Time-dependent geminal method applied to laser-driven beryllium,” Phys. Rev. A **97**, 013423 (2018).
 - [56] W. P. Reinhardt, “Complex coordinates in the theory of atomic and molecular structure and dynamics,” Ann. Rev. Phys. Chem. **33**, 223 (1982).
 - [57] M. Kotani, *Quantum Mechanics I* (Iwanami Shoten, Tokyo, 1951).
 - [58] M. Spanner and S. Patchkovskii, “One-electron ionization of multielectron systems in strong nonresonant laser fields,” Phys. Rev. A **80**, 063411 (2009).
 - [59] M. Spanner and S. Patchkovskii, “Molecular strong field ionization and high harmonic generation: A selection of computational illustrations,” Chem. Phys. **414**, 10 (2013).
 - [60] V. P. Majety, A. Zielinski, and A. Scrinzi, “Photoionization of few electron systems: a hybrid coupled channels approach,” New J. Phys. **17**, 063002 (2015).
 - [61] Q. Zhang, P. Lan, and P. Lu, “Empirical formula for over-barrier strong-field ionization,” Phys. Rev. A **90**, 043410 (2014).
 - [62] See Supplemental material at [link inserted by PRA] for a text file containing the static-field ionization rates obtained by the MCTDHF method for $2 \leq Z \leq 36$.
 - [63] S.-J. Yang, X.-S. Mei, T.-Y. Shi, and H.-X. Qiao, “Application of the Hylleraas-*B*-spline basis set: Static dipole polarizabilities of helium,” Phys. Rev. A **95**, 062505 (2017).
 - [64] H. Nakashima and H. Nakatsuji, “Solving the Schrödinger equation for helium atom and its isoelectronic ions with the free iterative complement interaction (ICI) method,” J. Chem. Phys. **127**, 224104 (2007).
 - [65] D. J. Haxton, K. V. Lawler, and C. W. McCurdy, “Multiconfiguration time-dependent Hartree-Fock treatment of electronic and nuclear dynamics in diatomic molecules,” Phys. Rev. A **83**, 063416 (2011).
 - [66] N. Moiseyev, P. Certain, and F. Weinhold, “Resonance properties of complex-rotated hamiltonians,” Mol. Phys. **36**, 1613 (1978).
 - [67] J. Bengtsson, E. Lindroth, and S. Selstø, “Solution of the time-dependent Schrödinger equa-

- tion using uniform complex scaling,” Phys. Rev. A **78**, 032502 (2008).
- [68] J. D. Jackson, *Classical Electrodynamics* (John Wiley and Sons, Inc., Hoboken, NJ, 1998).
- [69] F. C. Sanders and C. W. Scherr, “Perturbation study of some excited states of two-electron atoms,” Phys. Rev. **181**, 84 (1969).
- [70] A. Kramida, Yu. Ralchenko, J. Reader, and NIST ASD Team, NIST Atomic Spectra Database (ver. 5.7.1), [Online]. Available: <https://physics.nist.gov/asd> [2019, December 26]. National Institute of Standards and Technology, Gaithersburg, MD. (2019).